在追隨地勢座標下處理雙都普勒雷達資料求取一颱線系統的運動結構方法

鄧仁星　陳景森

中央大學大氣物理研究所

摘　要

本篇介紹一在山區利用雙都普勒雷達資料求取風場的改進方法，此方法是建立在追隨地勢座標以便得到較合理的垂直速度下邊界條件。

經由我們利用此改進方法（方法A）所得的風場與模式結果及以往建立在直角座標的處理方法（方法B）所得的比較中，可知在平坦地區方法A與方法B或方法A與模式結果之間幾乎沒有差別。但在地勢起伏較大區域時，方法A所得的風場與地形之間有較好的配合關係，上升及下降速度區分別發生在氣流爬坡及下坡的地方。

希望經由本篇所介紹的改進方法，對於往後利用都普勒雷達資料探討山區雲雨系統的研究有所助益。

四、環境風場與地形對降水系統之影響-非靜力雨雲模式之模擬探討

利用非靜力地形座標的雲雨模式，探討環境風場雨地形對降水系統的影響。我們以1987年6月20日台灣地區的衛星及雨量資料來分析降水系統的特性，這一天風向主要來自南方，但是北部地區有高於100 mm / 日的雨量，模擬結果發現北部的降水主要受到氣流在北部地區輻合而產生，再加上地面加熱降低自由對流高度(LFC)所以北部地區能夠有較大的雨量。模擬結果亦顯示風向如爲165°及225°則北部地區的降水會偏向西北及東北，因此如果能知道風向，則對降水發生的地區的預報有參考價值。詳細結果在附錄B 。

Reprint from Terrestrial, Atmospheric and Oceanic Sciences

Vol.5, No.2, 137-168, June 1994

On the Formation of Cloud and Precipitation Systems in Taiwan During TAMEX IOP #11

Ching-Sen Chen[1] *and Yuet-on E. Chan*[1]

[1]*Institute of Atmospheric Physics, National Central University, Chung-Li, Taiwan, R.O.C.*

TAO office: P.O. Box 23-59, Taipei, Taiwan, R.O.C.

TAO, Vol.5, No.2, 137-168, June 1994

On the Formation of Cloud and Precipitation Systems in Taiwan During TAMEX IOP #11

CHING-SEN CHEN[1] and YUET-ON E. CHAN[1]

(Manuscript received 26 October 1993, in final form 16 May 1994)

ABSTRACT

Mountains can provide heat and moisture to the atmosphere and act as a barrier to the prevailing wind. Thus they can influence the formation and development of precipitation systems. About two-thirds of the island of Taiwan is occupied by mountains. Therefore, it is important to understand the influence of terrain on the formation and development of precipitation systems. This kind of research has become one of the objectives of the Taiwan Area Mesoscale Experiment (TAMEX, Kuo and Chen, 1990) held in 1987.

On June 20, 1987 during TAMEX IOP 11, a Pacific high pressure system was over Taiwan. Two major precipitation systems occurred in the Taiwan area in the afternoon. According to satellite and surface data, one precipitation system was over northern Taiwan and the other over central Taiwan. Several soundings show that southern Taiwan was under the influence of southerly flow and northern Taiwan was affected by southwestern flow. The Pan-Chiao sounding in northern Taiwan indicates the level of free convection (LFC) decreased to 1 km in height at 1400 LST. Thus lifting due to topographic effects or other factors could help convection . A three-dimensional non-hydrostatic numerical model with terrain following coordinate system was employed to study where cloud systems developed. We found that when the initial wind used in the model was from the south, water vapour convergenced in northern Taiwan. Then cloud and rain formed there. The formation of this cloud and rain system plus surface heating helped to form a convergence area. The land-sea temperature contrast seemed not to be important for the formation of this convergence area, but it could enhance the intensity of the cloud system. If wind direction was from either 165° or 225°, the cloud and precipitation system formed in northwestern and northeastern Taiwan, respectively. Upslope flow helped clouds form in central Taiwan. The cloud and precipitation system formed in the mountainous area in central Taiwan when initial wind in the model was from 165°, 190°, and 225°. Higher wind speed from the south at low level would cause the precipitation in northern Taiwan to move northward away from Taiwan island rather than eastward as observation data indicated.

(Key words: Terrain, Cloud and Precipitation System, TAMEX)

[1] Institute of Atmospheric Physics, National Central University, Chung-Li, Taiwan, R.O.C.

1. INTRODUCTION

Mountains act as a heat and moisture source as well as a barrier to the prevailing wind. The moisture can influence the formation of precipitation systems. Kuo and Orville (1973) studied the mountainous storms over the Black Hill in South Dakota, U.S.A. They found that the prevailing wind could affect the position of the formation of mountainous storms. Karr and Wooten (1976) analyzed radar echoes over the Rocky Mountains. They found that mountain "hot spots" were favorable for the formation of radar echo. Banta and Schaaf (1987) used satellite data to trace where mountainous thunderstorms initially formed and found the initiation stayed on the lee side. The "lee side convergence zone" as favorable for the formation of cumulus clouds has also been proposed by Banta (1984).

As mountains occupy so much of the land-mass of Taiwan island (Figure 1), their effects on the formation of cloud systems and mountainous storms is very important. Liao and Chen (1984) presented two cases where storms formed in mountainous area in the afternoon and

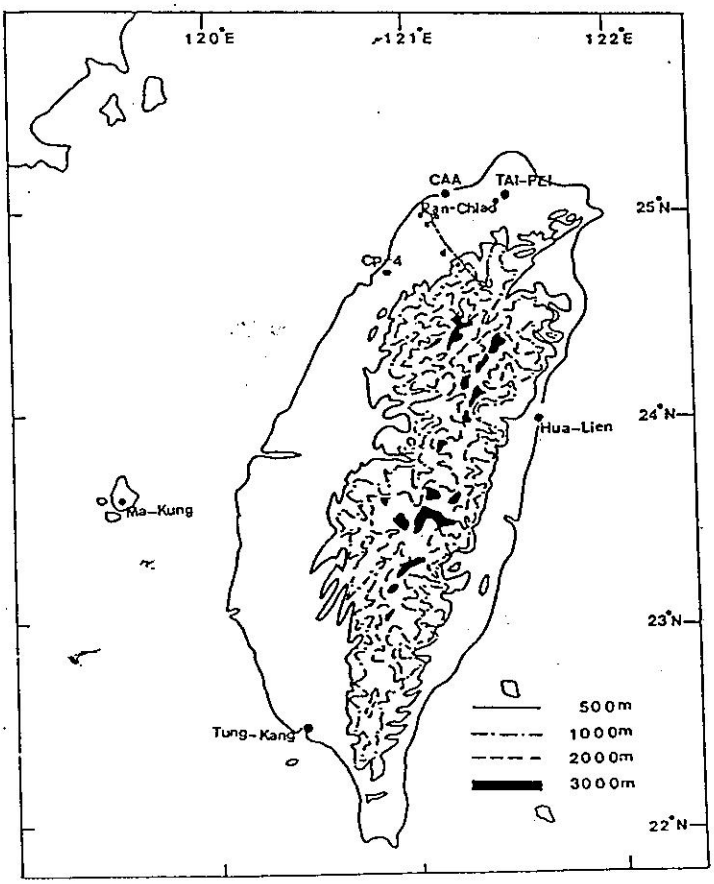

Fig. 1. The topography of Taiwan in meters. Stations along the broken-line will be mentioned in Figure 8.

then moved toward the Taiwan strait. Chen *et al.* (1991) studied a mountainous storm which formed in a mountain slope area in the afternoon in northern Taiwan and then moved eastward. This system dumped more than 100 mm of precipitation at some stations in only a few hours. The maximum reflectivity was over 50 dBZ along the steep slope and near the mountain peak. On June 20, 1987 during the TAMEX (Taiwan Area Mesoscale Experiment, Kuo and Chen, 1990) mountainous precipitation systems formed in northern and central Taiwan in the afternoon and then moved eastward (Figure 2). The pattern of daily rainfall amount (Figure 3) formed three groups. The magnitude of the rainfall amount was large in northern and central Taiwan, but less in the south. In northern Taiwan precipitation formed in early afternoon (Figure 4) but not in southern Taiwan. In southern Taiwan, some of the precipitation might come from cloud systems moving from the Taiwan strait (Figure 2).

The objective of this paper is to study why mountainous cloud and precipitation systems form in northern and central Taiwan in early afternoon as well as the important factors that help storms occur. To answer these questions, we will analyze conventional data as well as simulation results from a three-dimensional non-hydrostatic numerical model. We hope that after this study we shall have a better understanding of the formation of mountainous cloud and precipitation systems over Taiwan island.

The analysis of observational data will be described in section 2. The model structure will be presented in section 3 and appendix. The modeling simulation results will be discussed in section 4.

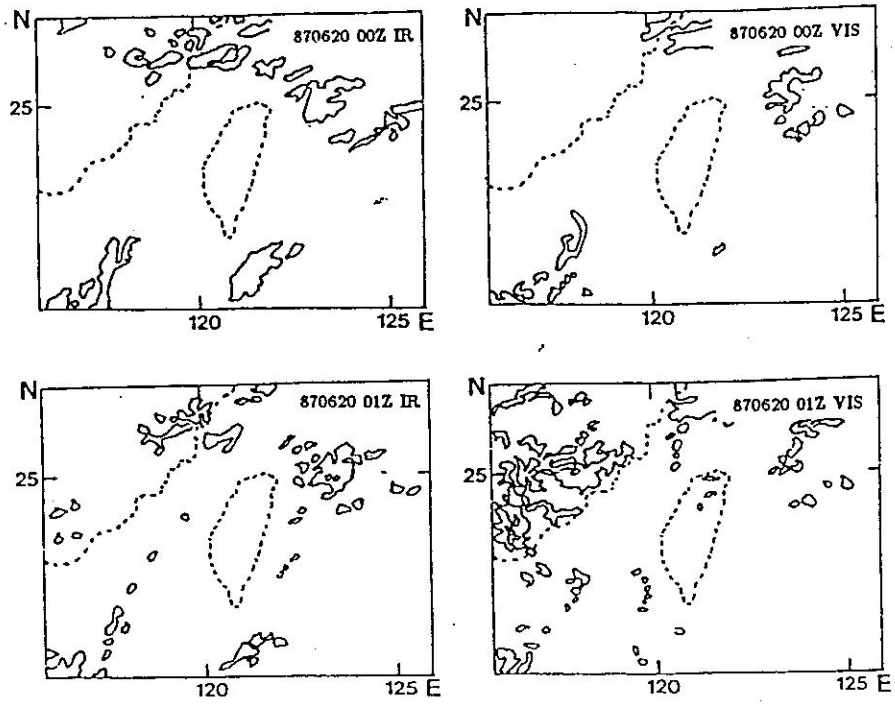

Fig. 2. Infrared (IR) and visible (VIS) satellite images from 0800 LST (00Z) to 1700 LST, 20 June 1987, dotted line is the coastline, solid line is the cloudy area.

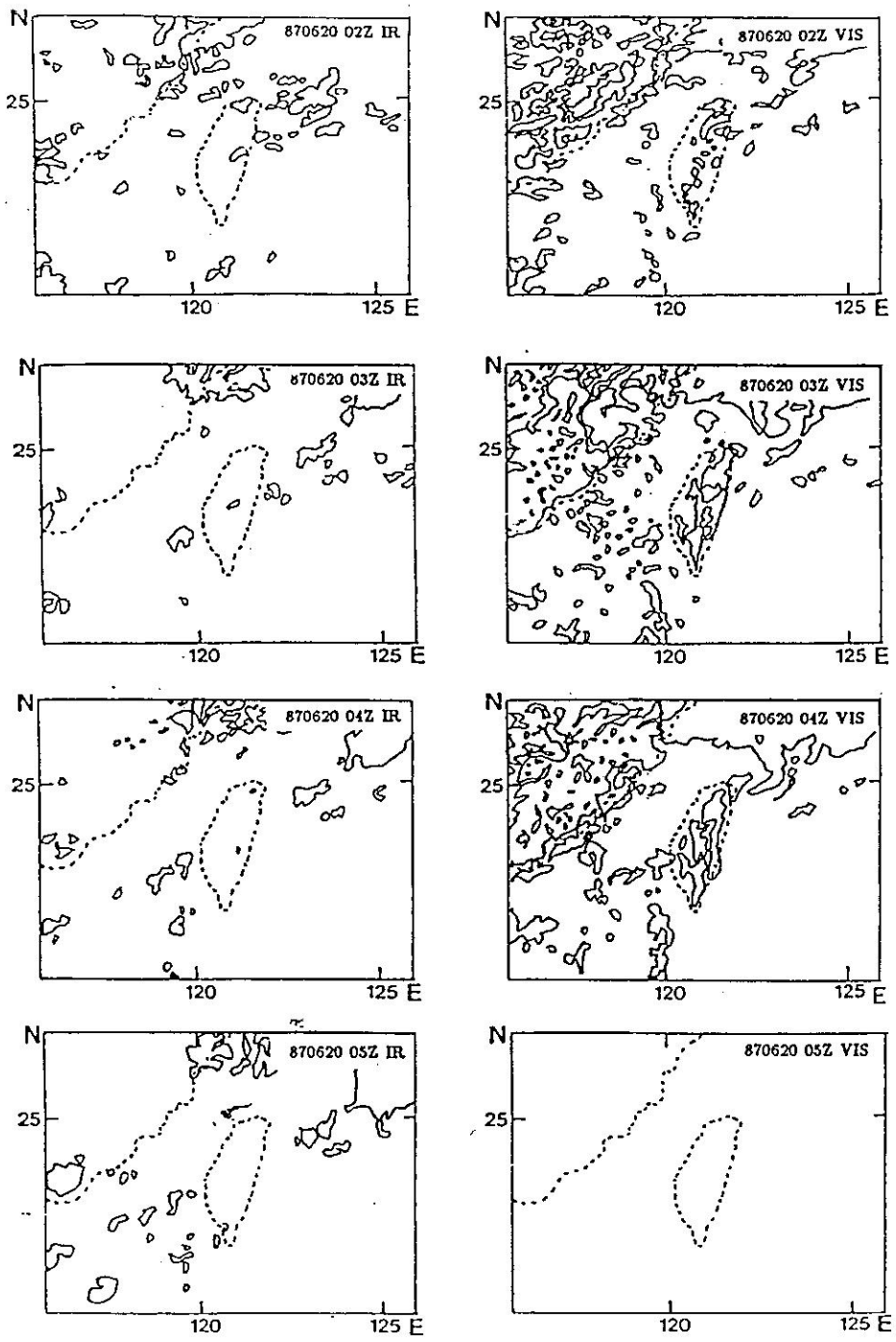

Fig. 2. (Continued.)

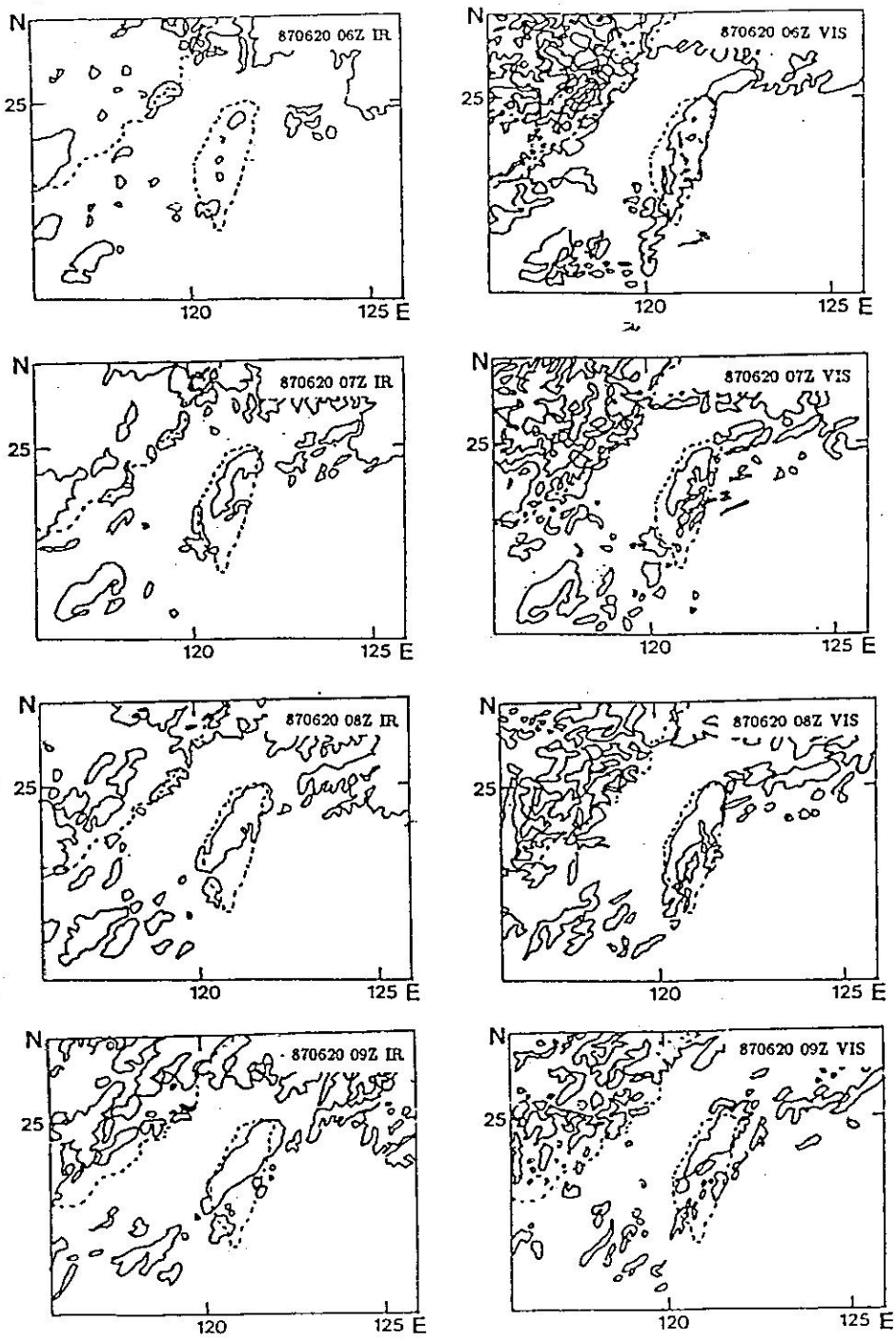

Fig. 2 (Continued.)

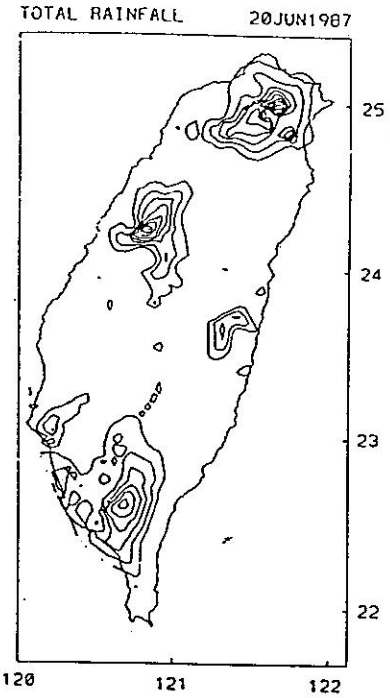

Fig. 3. The daily rainfall amount (mm) over Taiwan island on 20 June, 1987. The contour intervals are 10 mm starting from 10 mm to 70 mm.

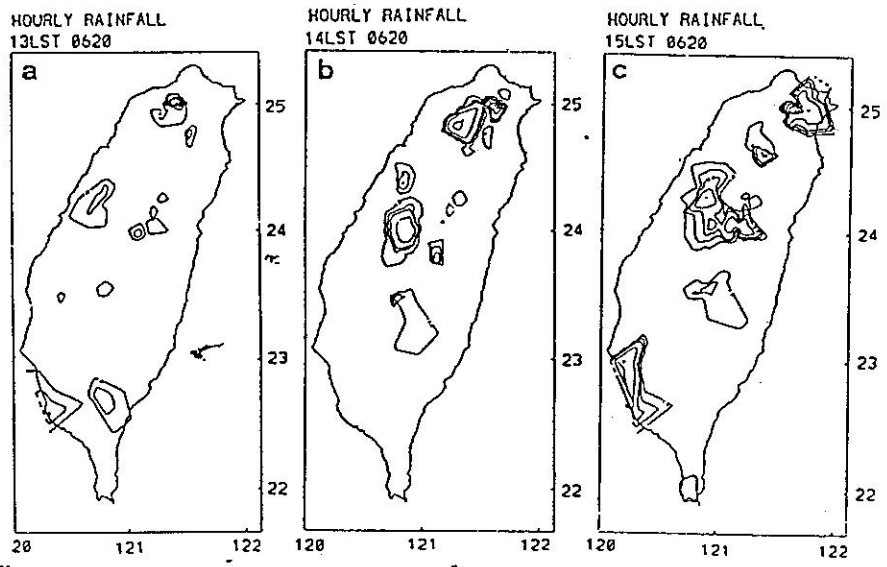

Fig. 4. The hourly rainfall rate (mm h^{-1}) at (a) 1300, (b) 1400, (c) 1500 LST on 20 June 1987. The contour intervals are 1, 3, 5, 10, 20, 30 mm, respectively.

2. DATA ANALYSIS

A surface weather map (Figure 5a) and satellite images (Figure 5b) show that a Mei-Yu frontal system was located some distance to the north of the Taiwan area on June 20, 1987 but a Pacific high pressure system influenced the Taiwan weather pattern. In southern Taiwan wind was from the south while in northern Taiwan southwest wind was found as it was located in the northern periphery of the high pressure system. The diurnal change of wind direction was very obvious as shown in Figure 6. Airflow moved away from Taiwan island at 0500 LST (local stand time) and converged on the island and mountainous areas at 1200 LST. Figure 7 depicts the hourly variation of wind, temperature, moisture and precipitation at Taipei and Pen-Chia-Yu stations. In Taipei wind direction changed from south (downsloped direction) to west (on-shore) and temperature increased after 0900 LST. These phenomena have also been observed by Johnson and Bresch, (1991). The temperature dropped and wind direction changed after 1300 LST due to precipitation (Figure 4). Wind direction changed

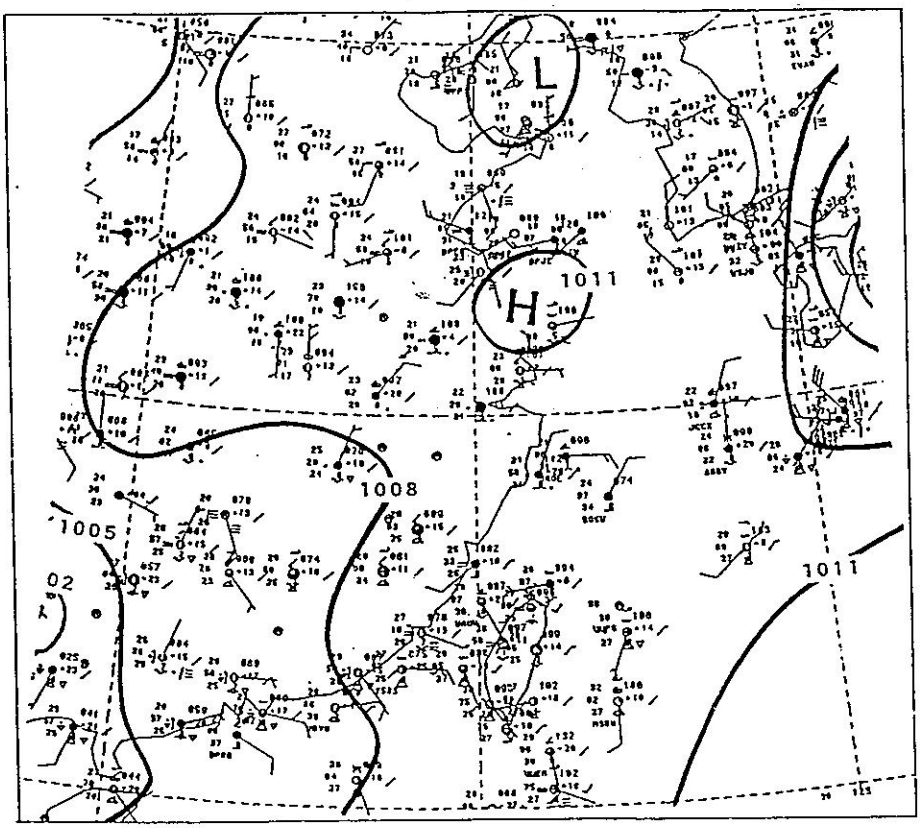

(a)

Fig. 5. (a) Synoptic-scale surface map and (b) Infrared satellite image for 0800 LST, 20 June 1987.

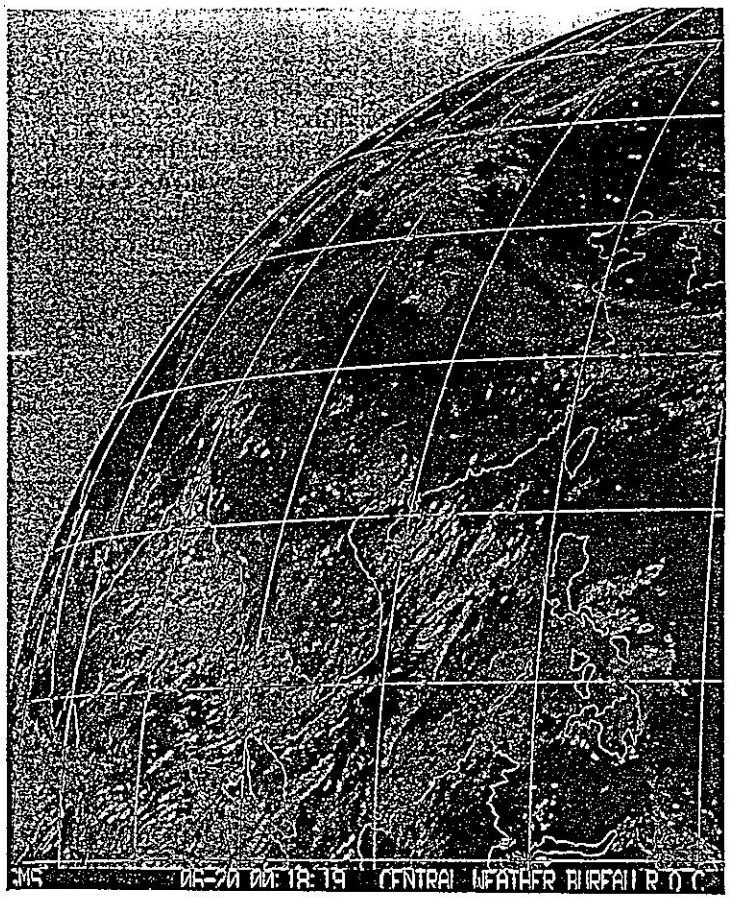

(b)

Fig. 5. (Continued.)

back to southerly wind at 1500 LST. In Pen-Chia-Yu wind changed to northerly at 1500 LST and southerly again at 1900 LST. Thus from these two stations, it is hard to say any mesoscale features related to front had reached northern Taiwan. Since the prevailing wind direction in southern Taiwan (Tung-Kang) was from the south (Figure 8), the change of wind direction in southern Taiwan was not so obvious as that in northern Taiwan (Figure 6). Figure 9 depicts the surface wind field along a line from the coast to the mountains in northern Taiwan (Figure 1). On-shore flow developed near the coast (a, b and c stations) between 0800 and 0900 LST. Along slope (d, e and f stations) upslope wind also developed between 0830 and 0930 LST. The upslope wind had a northerly wind component which was also found in Pan-Chiao in the afternoon (Figure 8). The direction of upslope wind depended on the terrain features around the station. Thus in northern Taiwan the on-shore flow and upslope flow developed almost at the same time. However due to lack of data, it was not easy to determine the development of upslope flow in other regions.

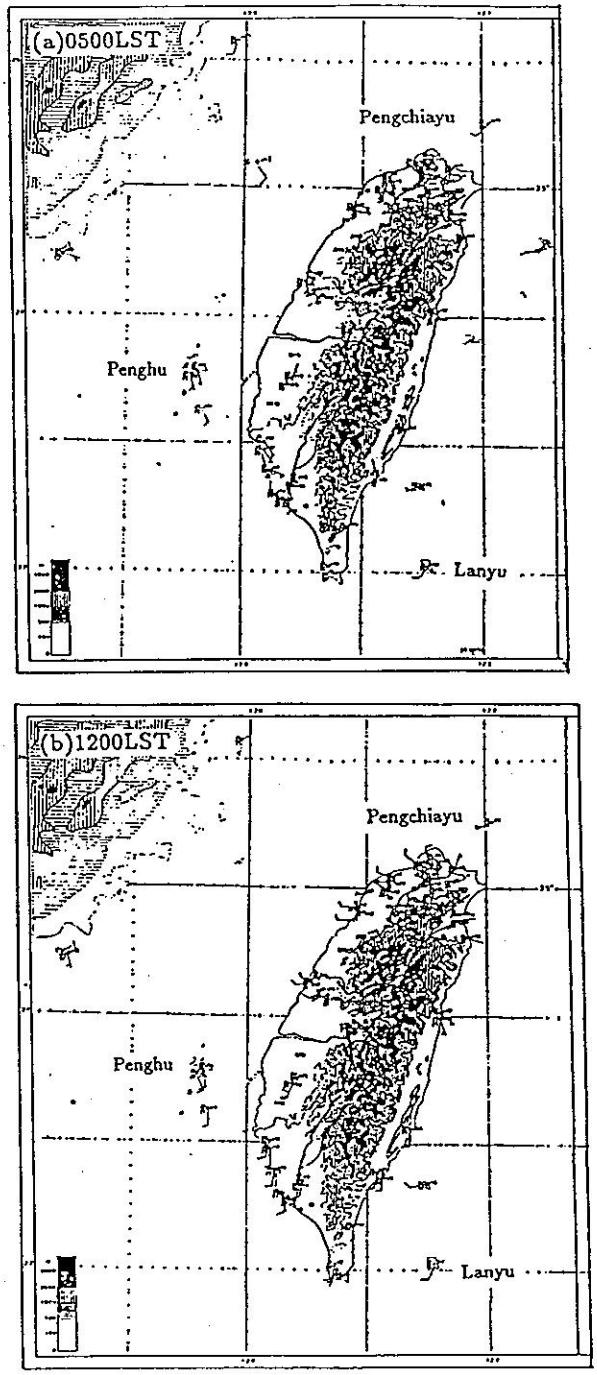

Fig. 6. Conventional meteorological variables on the surface for (a) 0500 LST and (b) 1200 LST on 20 June 1987 in the Taiwan area.

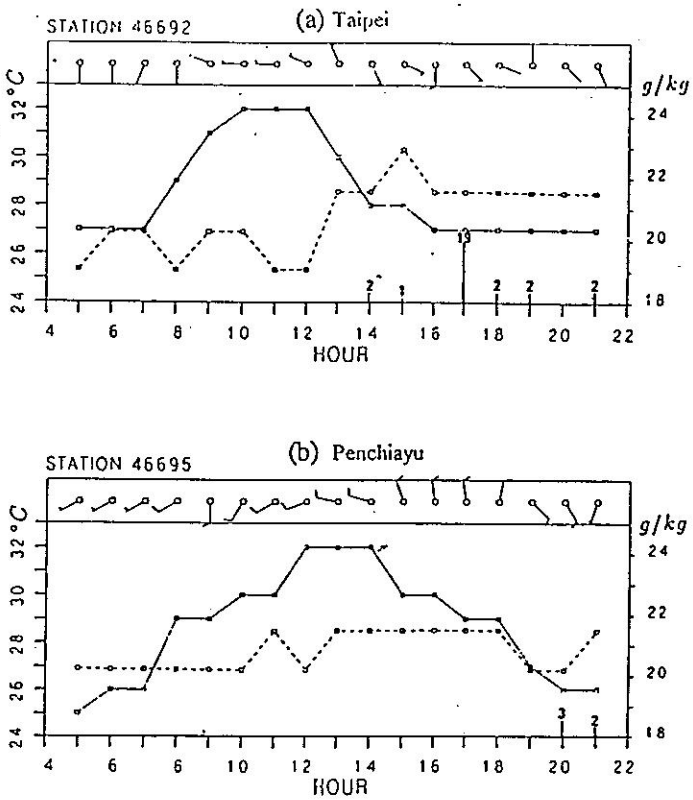

Fig. 7. The hourly wind, temperature (solid line), mixing ratio of water vapour (dashed line) and precipitation (bar, mm hr^{-1}) at Taipei (a) and Pen-Chia-Yu (b).

The vertical potential temperature, equivalent potential temperature and saturated potential temperature profiles at 0800, 1100 and 1400 LST at Pan-Chiao station in northern Taiwan are shown in Figure 10. In the early morning the atmospheric was near neutral on the low levels. After the sun rose, low level temperatures increased as seen for 1100 and 1400 LST. The level of free convection (LFC) was reduced to about 1 km in height in the afternoon, therefore the lifting due to topographical effects or other mechanisms was expected to help air parcels at low level to rise and to form cloud and rain. This situation was confirmed by surface rainfall data (Figure 4). Hourly surface rainfall data indicated that significant rainfall amounts began in the Taipei area in northern Taiwan and central Taiwan at 1300 LST (Figure 4). there was 79 mm/$hour^{-1}$ at one station. But the amount of rainfall was less at other stations. In central Taiwan rainfall began in the slope area and higher mountain regions. Radar reflectivity also indicated this situation (See Figure 10 of Liang, 1991). The amount of precipitation was smaller than that in northern Taiwan in the early afternoon. At 1400 LST more stations observed precipitation, but still in northern and central Taiwan. In northern Taiwan more stations east of Taipei observed precipitation, which indicated that precipitation formed in northeastern Taiwan. At 1500 LST this phenomena become more evident. Meanwhile, the rainfall intensity in central Taiwan also became heavier in the mountainous area.

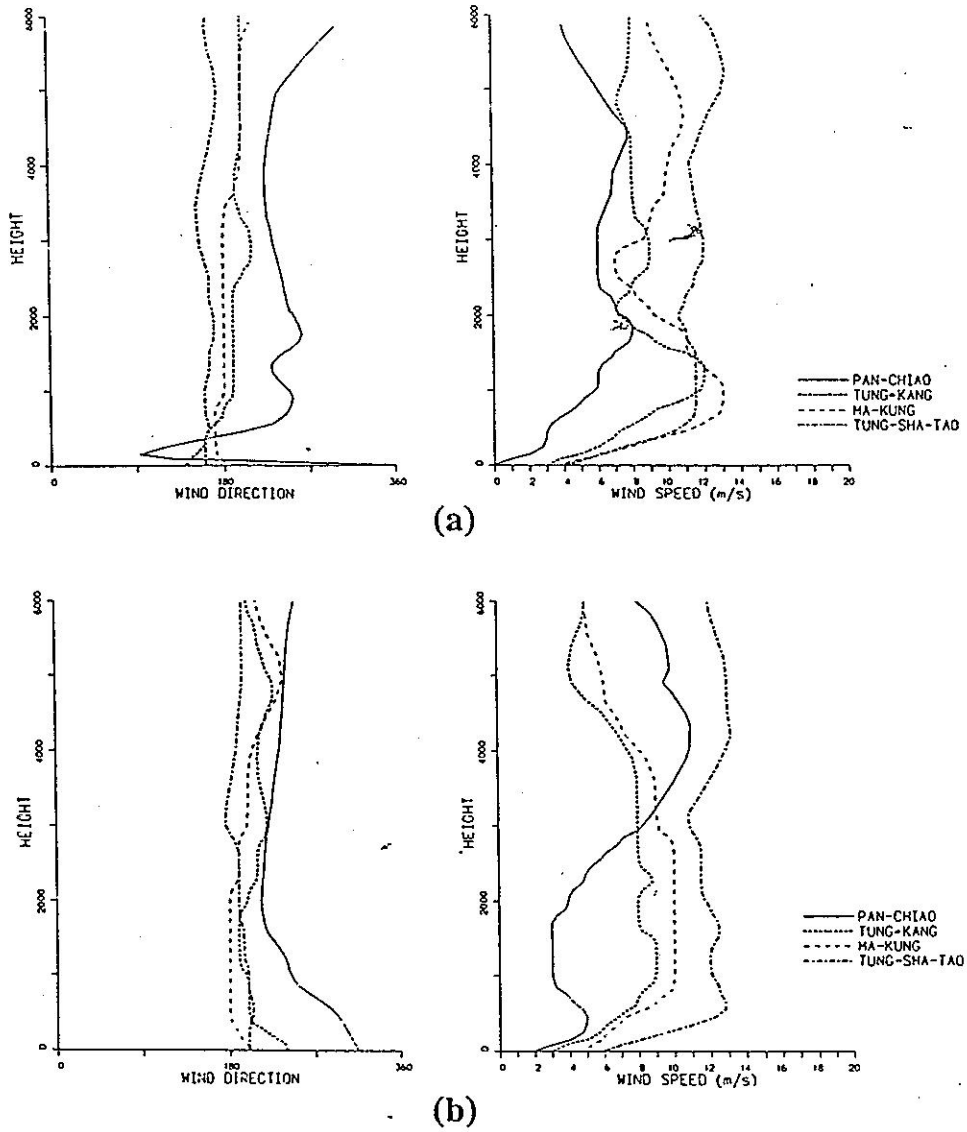

Fig. 8. The vertical profile of wind direction and speed over Pan-Chiao, Tung-Kang, Ma-Kung and Tung-Sha-Tao at (a) 0800 LST and (b) 1400 LST on 20 June, 1987.

Observations indicate that a Pacific high pressure system influenced Taiwan weather on June 20, 1987. The sea-breeze and upslope wind developed after 0800 to 0900 LST in a region of southerly wind. The Pan-Chiao sounding showed that the height of the LFC decreased to 1 km in the afternoon and thus precipitation formed more easily with the help of terrain lifting. Hourly rainfall data showed that major precipitation occurred in northern

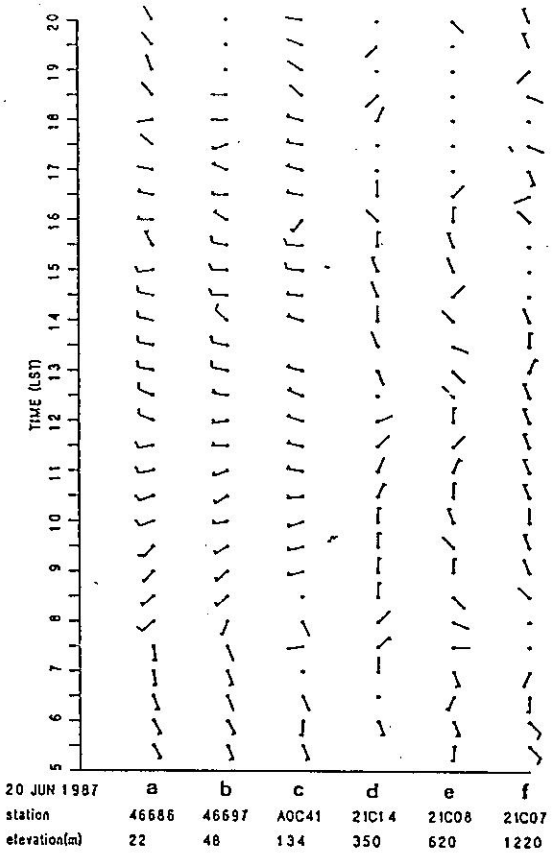

Fig. 9. Hourly change in wind direction at station (a) CKS Airport, (b) Tao-yuan, (c) Chung-li, (d) Hsia-yun, (e) Kao-I, (f) Pa-leng. The position of these stations is shown in Figure 1.

and central Taiwan at 1300 LST. As time possed, precipitation took place east of Taipei in northern Taiwan. Two areas had precipitation in central Taiwan. One was along the slope and the other over high mountains.

3. MODEL STRUCTURE

The numerical model used in this study was a finite-difference approximation of the elastic, non-hydrostatic equations governing atmospheric motion. This model utilized the compressible equations, which were efficiently solved by separating out sound wave terms and integrating them with a smaller time step than that used for the convective processes in order to maintain computational stability. The predicted variables included horizontal and vertical velocities, pressure, potential temperature (θ), the mixing ratio of water vapor (q_v), of cloud water (q_c) and rainwater (q_r). Cloud water and rainwater growth were parameterized in the manner suggested by Kessler (1969), but with the coefficients used by Klemp and

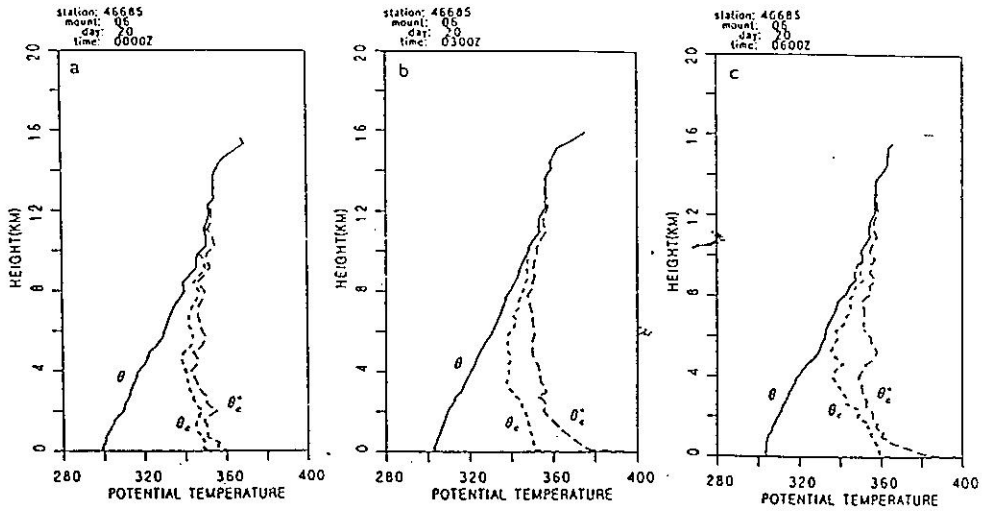

Fig. 10. The vertical profile of potential temperature, equivalent potential temperature and saturated equivalent potential temperature at (a) 0800 LST, (b) 1100 LST, and (c) 1400 LST at Pan-Chiao in northern Taiwan.

Wilhelmson (1978). The subgird scale parameterization used in this study followed Lilly's formulation (1962), which depended on the relative strengths of stratification and shear.

The boundary conditions of the velocity components for the upper and lower boundaries were assumed to have zero normal velocity and zero normal velocity gradient conditions for horizontal velocities. There was also no normal gradient for θ, q_v, q_c, and q_r at the boundaries. In the upper half of the model domain, a region of Rayleigh friction and Newtonian cooling were applied to the perturbation velocities and θ. The lateral boundary conditions were assumed to have no horizontal gradient at the inflow boundaries, but Orlanski (1976) type conditions were employed for the horizontal velocities of the outflow boundaries.

The numerical scheme used in the model was similar to that of Durran and Klemp (1982). The model domain is 400 km×800 km×10 km. The horizontal grid interval was 10 km and the vertical grid interval varies from 173 m near the surface to 642 m near the top. The big time step was 4 seconds and the small time step was 1 second. Smooth terrain with mountain peak 3 km in height was assumed in the model (Figure 11). A brief description of the model structure is presented in the Appendix.

4. SIMULATION RESULTS

To choose the initial wind profile used in the model is rather difficult. Since northern Taiwan was located in the northern periphery of a high pressure system, the wind direction in Pan-Chiao (northern Taiwan) was from the southwest while in southern Taiwan (Tung-Kang) as well as over sea (Ma-Kung and Tung-Sha-Tao) wind direction was in general from the south (Figure 8). Thus in the model we assumed that the initial wind direction was either from 190° (case A, Table 1), 165° (case B) or 225° (case C). In Pan-Chiao (Figure 8) wind speed increased from the surface to 2 km in height (in the morning) or 4 km in height (in

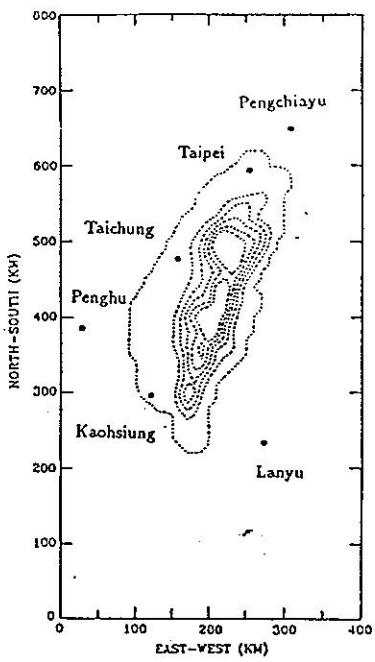

Fig. 11. The smooth terrain used in the model. Contours intervals are 500 m.

the afternoon). At other stations, wind speed was rather unchanged with height above 1 km. Since we were interested in the formation of the cloud and precipitation system in northern and central Taiwan, we assumed that wind speed was to be 0 ms^{-1} at surface and linearly increased to 8 ms^{-1} at mountain top (3 km high) in case A, B, C and E (Table 1). The temperature and moisture profiles were taken from Pan-Chiao data at 0800 LST. In run D, the wind direction was the same as in run A but wind speed at the mountain top was assumed to be 5 ms^{-1}. In run E the wind direction and speed were the same as in run A, but assumed to have no sea-land contrast. In case F we assumed that wind speed increased from 0 ms^{-1} at surface to 8 ms^{-1} at 1 km in height linearly and wind was from 190°. This wind speed profile was close to that observed in Tung-Kang in the afternoon (Figure 8). To avoid a big shock in the model, initially the wind speed was to be zero everywhere in the model and then slowly increased to its environmental value assumed in the model in the first three hours. Then we let the model to run for another hour. At 4 hours of simulation time the surface heating was activated to the lowest level over the land for another two hours. The heating added to the model was similar to that in (Banta, 1986). During this time the surface temperature could increase about 2°K over the plain in the model which was close to the observed value for the maximum temperature variation at 1300 LST.

The surface streamline for run A at 4 hours of simulation time is shown in Figure 12. Airflow coming from the south was diverted near the southern tip of Taiwan and then followed the terrain contours. It again converged in northern Taiwan. The "H" and "L" in Figure 12 represent the local high and low pressure centers, respectively. They were located near the upstream and lee sides of the mountain, respectively. Perturbation high pressure area corresponded to the upward motion. These flow features were similar to those in Lin

Table 1. Experiments described in the numerical simulation.

Case	Comments
Run A	Wind direction is 190° and wind speed is linearly increased to 8 ms^{-1} at the mountain top (3 km in height). Wind speed is kept 8 ms^{-1} above 3 km in height. Temperature contrast is assumed between sea and land surface.
Run B	Same as in Run A but initial wind direction is 165°.
Run C	Same as in Run A but initial wind direction is 225°.
Run D	Same as in Run A but maximum wind speed is 5 ms^{-1} at mountain top.
Run E	Same as in Run A but no sea-land temperature contrast.
Run F	Same as in Run A but wind speed is linearly increased to 8 ms^{-1} at 1 km in height and then kept at 8 ms^{-1} above 1 km in height.

et al. (1992), however a stagnation point forms upstream of the island in our simulation result. This difference might be due either to the lower Froude number or the non-hydrostatic effect in our simulation model. How the flow with or without the stagnation point influenced the formation of cloud and precipitation systems needs further investigation. Since airflow converged in northern Taiwan, the increase of water vapor could have been expected. Figure 13 shows the mixing ratio of water vapor at 10 min after 4 h of simulation time if cloud and rain were suppressed. There existed a maximum region of the mixing ratio of water vapor in northern Taiwan. Thus cloud and rain systems can be expected there. At 4.5 hours, after surface heating was added for 30 minutes, airflow from the western, northern and eastern coastal line met the southerly wind forming a convergence zone in northern Taiwan (Figure 12b) over which there was a cloud and rain system (Figure 14a). The updraft of the cloud and rain system would enhance the low level convergence. The maximum value of cloud water in a vertical column is shown in Figure 14. Less cloud occurred in central Taiwan along the western slope region, where the area with upward motion in the upslope flow regime was small. Upward motion was also found in the eastern slope area in central Taiwan, but no cloud took place at this time. At 5 hours of simulation time, the convergence area moved slightly northward (Figure 12c) and major upward motion area shifted eastward in northern Taiwan but the updraft areas in central Taiwan remained in the same regions at this time and later. The cloud cover area in northern Taiwan remained roughly unchanged but it decreased in central Taiwan (Figure 14b). At 5.5 hours, the convergence area in northern Taiwan formed a line roughly parallel to the coasted line (Figure 12d) and the cloudy area in northern Taiwan extended to the northeast (Figure 14c). A small cloudy area formed on the eastern slope area and in the mountainous area in central Taiwan where upward motion also existed. Figure 15. shows the mixing ratio of rainwater at several horizontal planes and in an interior structure with a quarter cutout. Near surface rain was near the slope area. At higher levels it extended northward due to the southerly wind. The maximum mixing ratio existed at 5 $\sim$ 6 km height. At 6 hours (2 hours after heating was activated), several small scale features appeared in the surface flow pattern (Figure 12e). The cloud still covered northeastern Taiwan (Figure 14d) and intensified in mountainous areas in central Taiwan.

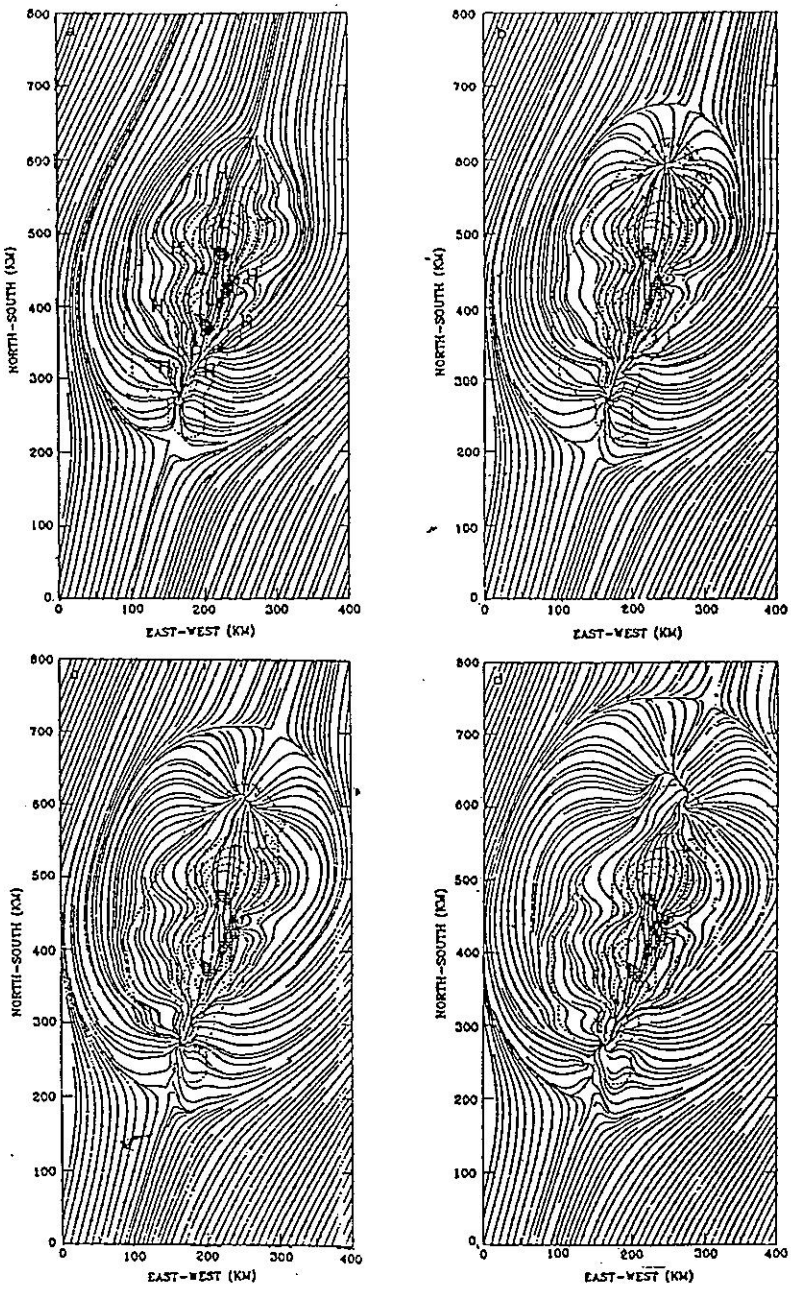

Fig. 12. Surface streamline for run A at (a) 4 hours, (b) 4.5 hours, (c) 5 hours, (d) 5.5 hours, and (e) 6 hours of simulation time. The dotted area and hatched area represent upward motion greater than 1 and 5 cm s^{-1}, respectively. H and L in (a) denote the maximum pressure and minimum pressure perturbation, respectively.

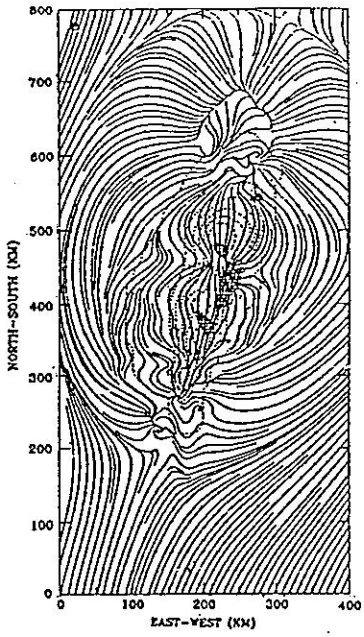

Fig. 12. (Continued.)

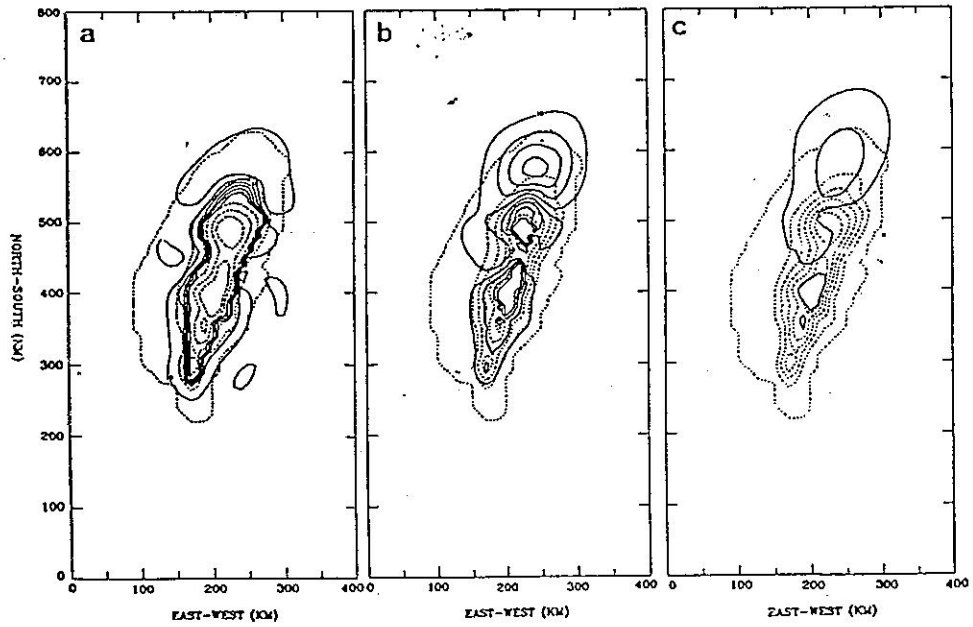

Fig. 13. The mixing ratio of water vapor at (a) 1 km (b) 2 km (c) 3 km height at 4 h 10 mins simulation time. Contour intervals are 3 g kg^{-1}.

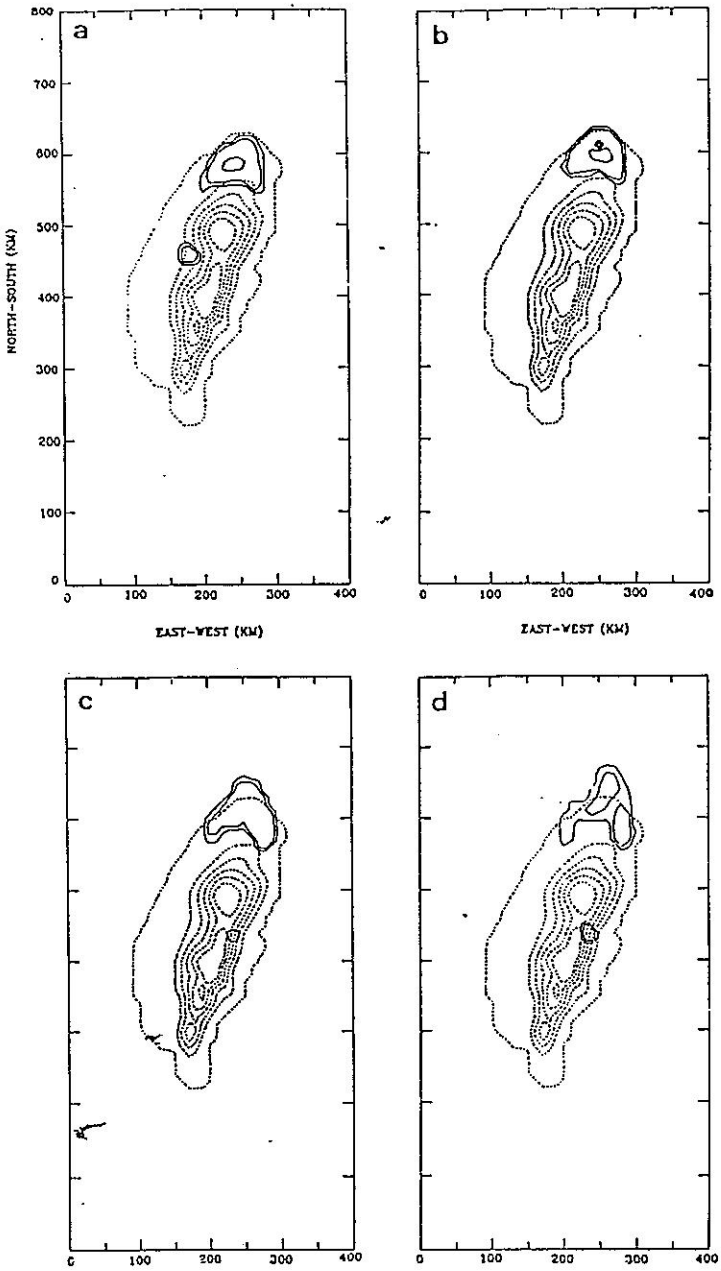

Fig. 14. The maximum value of the mixing ratio of cloud water in a vertical column for run A. The contour intervals are -2, -1, and 0 respectively. They represent 10^{-2}, 10^{-1}, and 10^{0} g kg^{-1}. The simulation time for each panel are at (a) 4.5 hours, (b) 5 hours, (c) 5.5 hours, and (d) 6 hours, respectively.

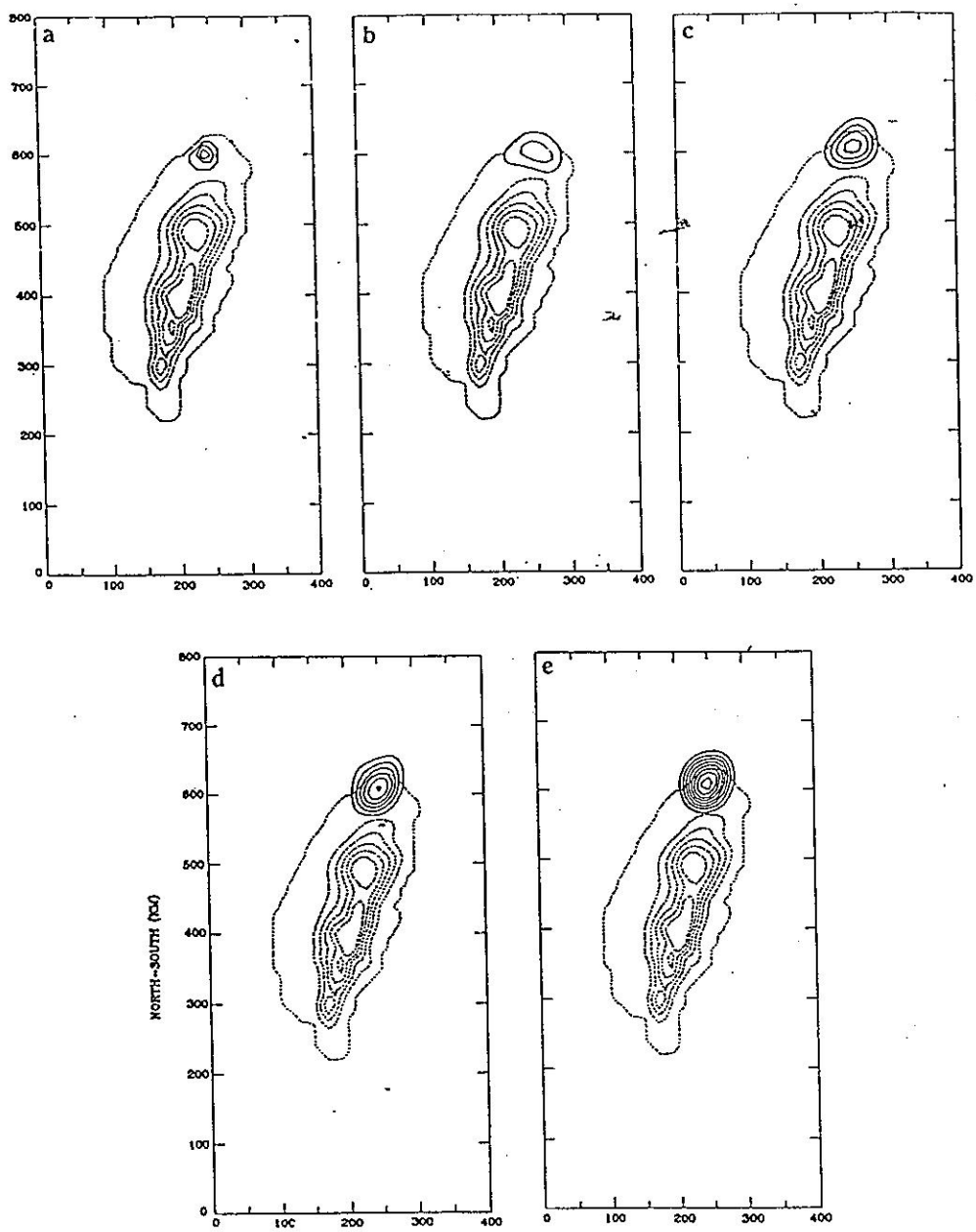

Fig. 15. The mixing ratio of rain water at (a) 1 km, (b) 2 km, (c) 3 km, (d) 4 km, (e) 5 km height at 5.5 hours. The contour interval is 1 g kg^{-1} except at 1 km, where it is 0.01 g kg^{-1}. The mixing ratio of rain in an interior structure with a quarter cutout superimposed with surface wind is shown in (f).

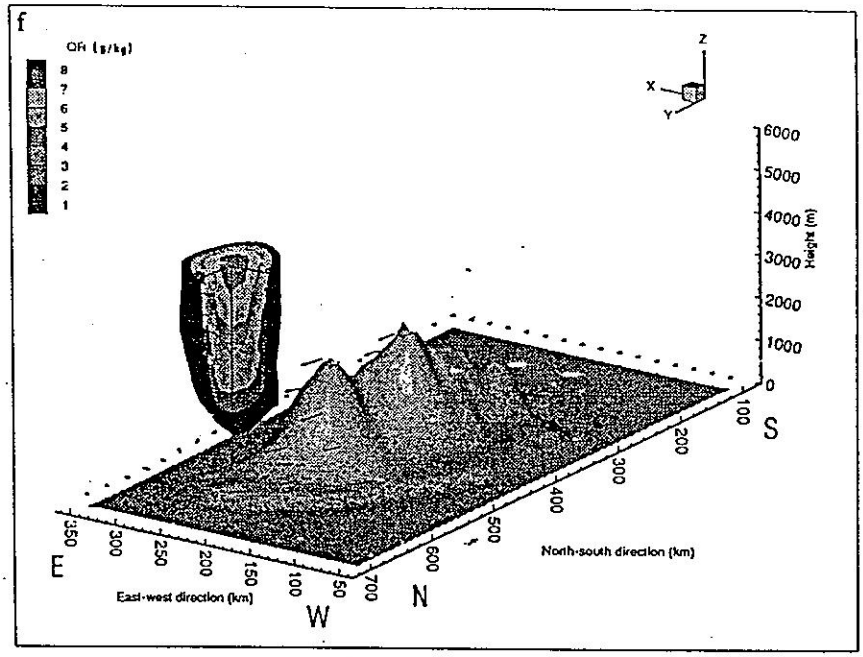

Fig. 15. (Continued.)

Since the convergence of the water vapor existed in the northern Taiwan for at least two hours, cloud and rain systems could develop in the conditional unstable atmosphere. The maximum value of the maximum radar reflectivity in a vertical column estimated from model result in northern and central Taiwan separately is shown in Figure 16. The formula to calculate the radar reflectivity from mixing ratio of rain water was adapted from Fovell and Ogura (1988). The maximum reflectivity was greater than 50 dBZ in northern Taiwan for about 2 hours. This situation corresponded to a higher rainfall rate in northern Taiwan. In central Taiwan the radar reflectivity was small. The upward area associated with the cloud in the upslope region was small in central Taiwan. Since major upward motion occurred in the slope area or mountainous area where the altitude was higher, the low level air parcel obtained less positive area once it passed its LFC (Figure 10). Thus the radar reflectivity was smaller.

In run A, clouds formed in northwest and northern Taiwan first, later extending to northeastern Taiwan. The intensity of radar reflectivity estimated from the model was higher. These phenomena were similar to the movement of the rainfall system (Figure 4). However for central Taiwan model results showed that only small cloudy areas formed on the western slope and in the mountainous areas. The intensity of cloud water and rain water was smaller in the model, as observation indicated. The upslope flow in northwestern Taiwan seen from the observations (Figure 8) was found only at 4.5 hours in run A (Figure 12b) and not obvious at other times.

In run B, the initial wind was from the southeast. Major cloud and rain systems formed in northwest and central Taiwan over areas of lower elevation and then moved north-westward away from the island (Figure 17). Stationary cloud also formed in the mountainous area of

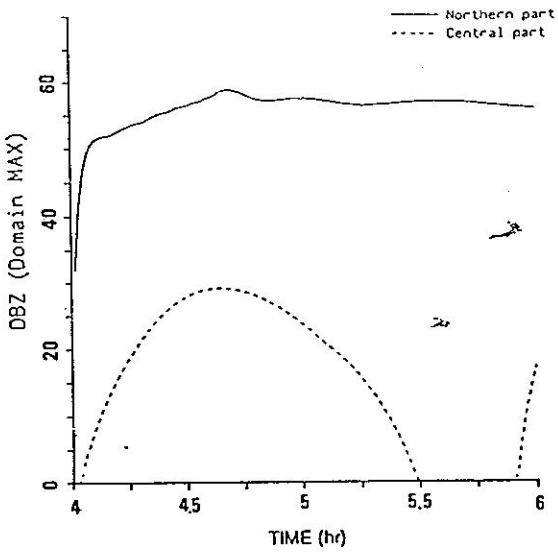

Fig. 16. The variation of the maximum value of maximum radar reflectively in a vertical column in northern and central Taiwan with time, respectively.

central Taiwan. This system was larger than that in case A. Although no large cloud cover formed over northeastern Taiwan, the movement of the cloud system looked similar to that of a cloud system under the influence of southeasterly wind studied by Liao and Chen (1984).

In run C, the initial wind was from the southwest and the model size was extended 100 km westward to move the boundary further away from Taiwan island. Major cloud and rain systems formed in northeastern Taiwan and moved northeastward away from the island (Figure 18). Stationary clouds also formed in mountainous areas in central Taiwan but with larger area coverage than that in case A. A small cloudy area also formed in southwestern Taiwan.

In run D, the wind direction was the same as that in run A but the initial wind speed was reduced to 5 ms^{-1} at and above the mountain top. The cloud and rain system can be found in Figure 19. In general the surface flow pattern in run D was similar to that in run A (not shown) but the convergence zone in northern Taiwan moved slowly northward. Thus the wind direction was from the north in northwestern Taiwan as seen from observed data before 5 h into the simulation (Figure 9). The cloud system in run D in northern Taiwan was similar to that in run A but remained slightly south of that in run A. Cloud formed in the central mountainous area in run D earlier than in Run A and enlarged at 6 hours of simulation time.

In run E, surface heating was applied to the lowest level over the whole domain. Thus there was no land-sea contrast in terms of surface property. The surface streamline looked similar to that in run A before 5.5 hours but some differences existed later (Figure 20a). For example, the flow direction in run A (Figure 12) was from the south in southwest Taiwan but in run E there was southeasterly wind over southwestern Taiwan. In northwestern and northeastern Taiwan, flow direction was more perpendicular to the coastline in run A than in run E. Upward motion was higher in run A. In the mountainous areas in central Taiwan, larger convergence, occurred in run A than in run E due to an easterly flow . In run E

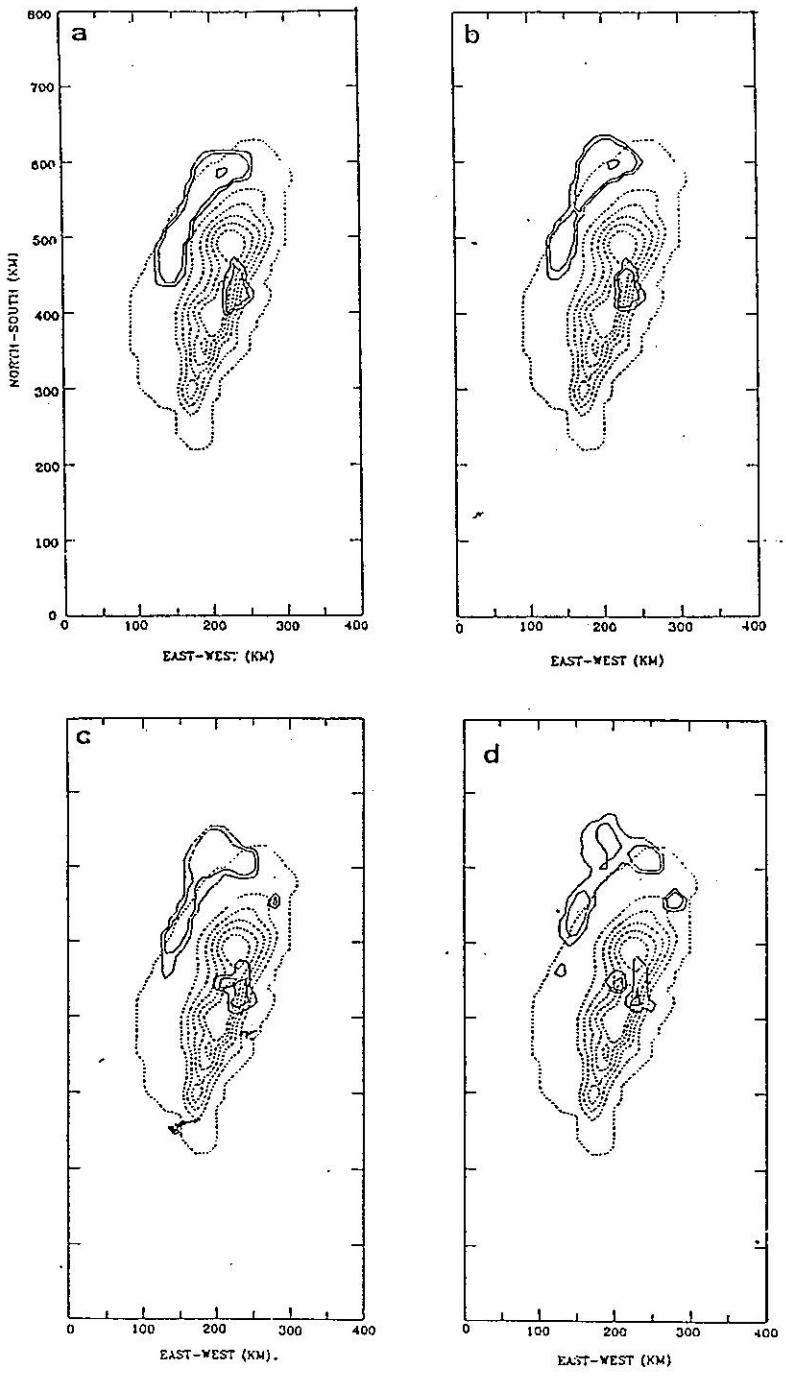

Fig. 17. Same as in Figure 14 but for run B.

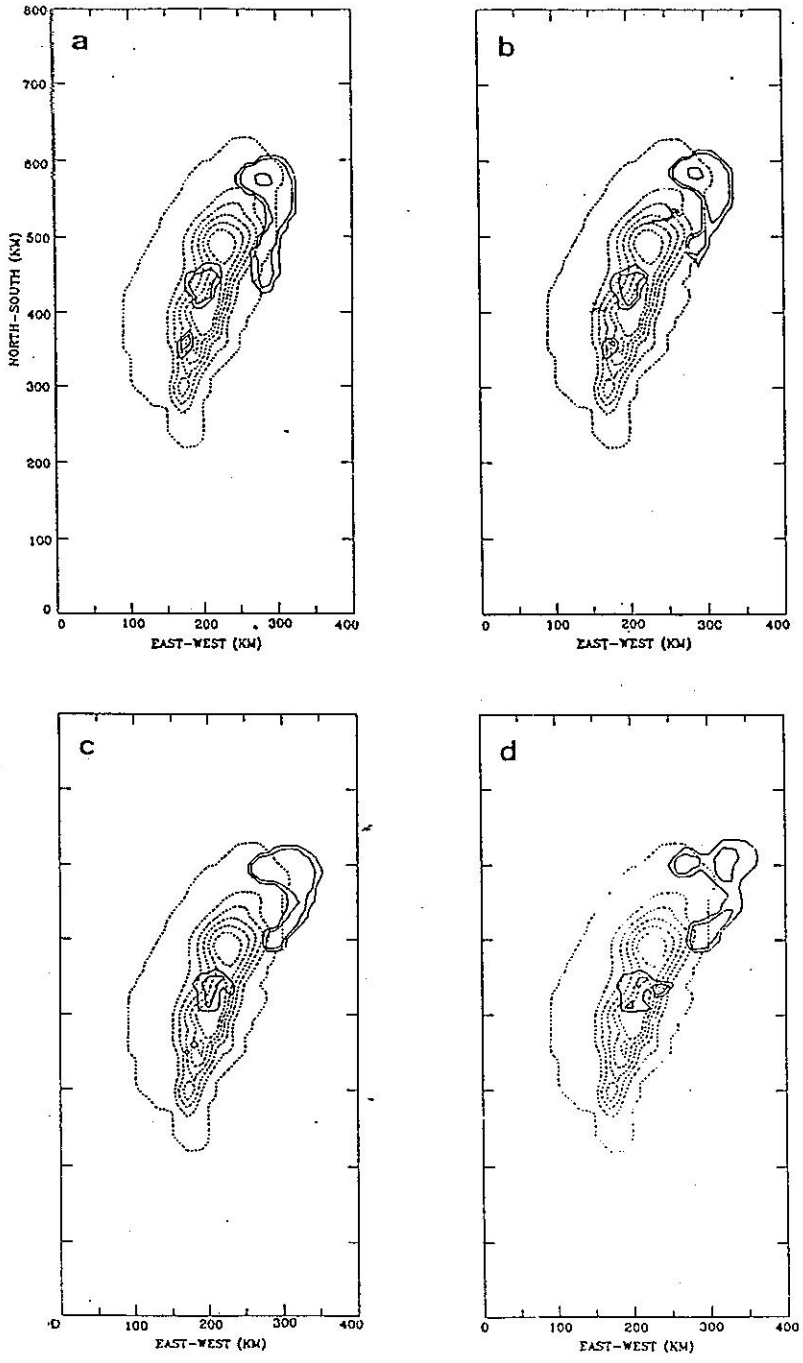

Fig. 18. Same as in Figure 14 but for run C.

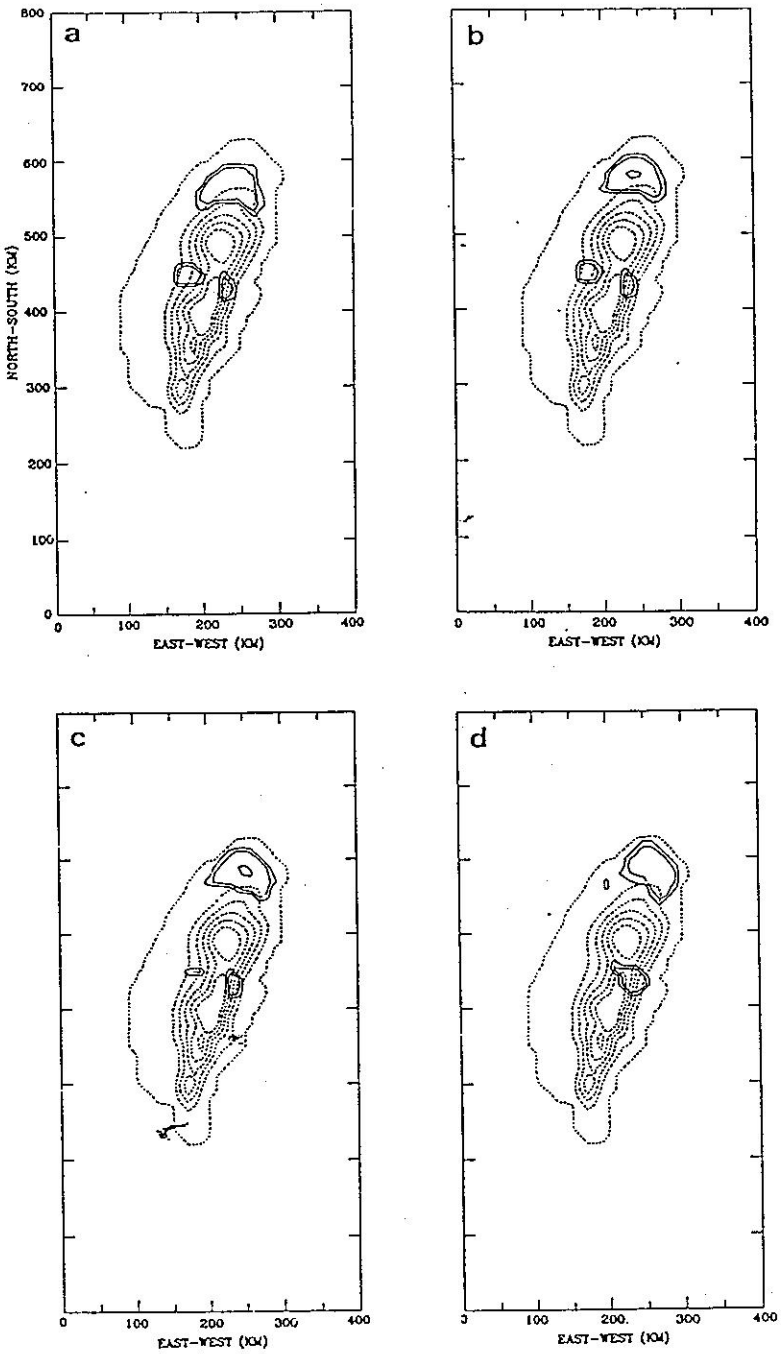

Fig. 19. Same as in Figure 14 but for run D.

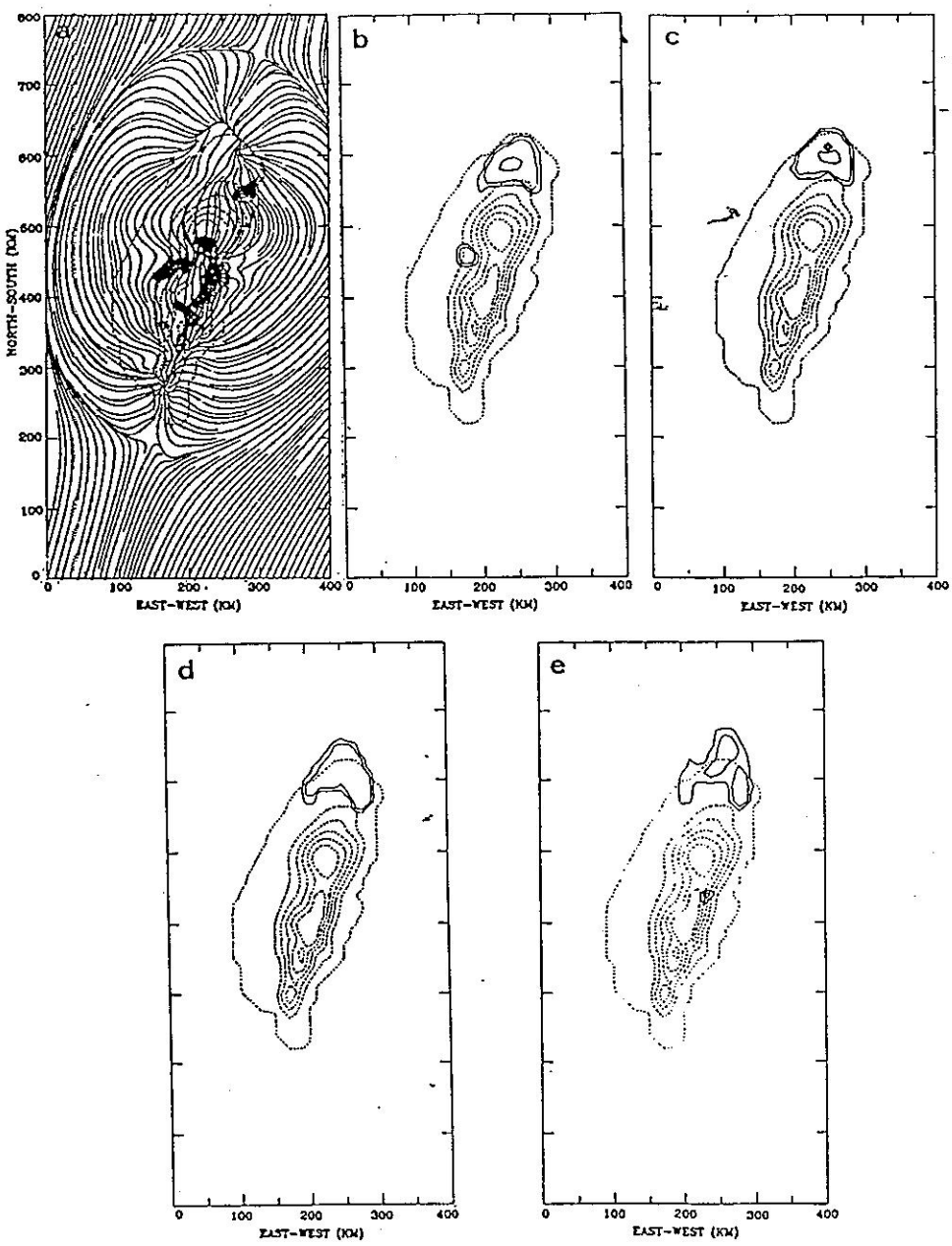

Fig. 20. (a) surface streamline at 5.5 hours of simulation time for run E. The dotted area and hatched area represent upward motion greater than 1 and 5 cm s^{-1}, respectively. The maximum value of the mixing ratio of cloud water in a vertical column for run E at (b) 4.5 hours, (c) 5 hours, (d) 5.5 hours, (e) 6 hours of simulation time.

the cloud and rain pattern in northern Taiwan (Figures 20b, c, d and e) was similar to that in run A but was weaker in central Taiwan.

The cloud pattern in run F (Figure 21) indicated that cloud formed in northern Taiwan and moved northward away from Taiwan island which is not consistent with observation (Figures 2 and 4). The cloud and rain system in central Taiwan was larger than that in run A. Observation (Figures 2 and 4) did not show that a large cloud system formed in the central Taiwan in early afternoon. The stronger cloud and rain system might be due to either the high wind speed assumed in the model or to the poor parameterization of cloud and rain water in the model.

From run A to run F, we found that cloud and rain system formation in northern and central Taiwan was principally due to the interaction between environmental wind and mountains in an environment with lower LFC when surface heating was activated. The convergence of the water vapor and heating effect caused the formation of a cloud and rain system in northern Taiwan. Upslope motion was responsible for the formation of the cloud and rain system in the slope area in central Taiwan. The land-sea temperature contrast could enhance the intensity of the cloud system through the increase in the strength of the convergence area in northern Taiwan and the mountainous area in central Taiwan. The wind direction assumed in the model could determine where cloud and rain systems formed in northern Taiwan. But cloud formed in the mountainous area when the wind direction was either 165°, 190° or 225°. There were also cloud and rain in northern Taiwan in run D when the wind speed was weak but the cloud and rain area were located slightly to the south when wind was stronger. In run F a cloud and rain system also formed in northern Taiwan in the stronger higher low-level wind-speed environment. But the precipitation system moved northward away from Taiwan rather than eastward as observational data indicated.

5. CONCLUSIONS

On June 20, 1987 during TAMEX IOP 11, a Pacific high pressure system was over Taiwan. Two major precipitation systems occurred in the area in the afternoon. According to satellite and surface data, one precipitation system was found over northern Taiwan and the other was over central Taiwan in early afternoon. The southern Taiwan area was under the influence of a southerly flow and northern Taiwan was affected by a southwest flow. The level of free convection (LFC) decreased to 1 km in height at 1400 LST as seen from Pan-Chiao sounding (Figure 10), thus lifting from the topographical effects or other factors could help convection occur. A three-dimensional non-hydrostatic numerical model with a terrain following coordinate system was employed to study where cloud systems occurred in the Taiwan area. We found that when the initial wind used in the model was from the south, water vapor converged in northern Taiwan. This caused the formation of cloud and rain systems. The updrafts of this cloud and rain system plus the surface heating effect helped to form the convergence area in northern Taiwan. The land-sea temperature contrast seemed not to be important for the formation of this convergence area, but it could enhance the intensity of the cloud and rain system through the increase of the convergence area. Upslope flow helped cloud form in central Taiwan. The cloud and rain could form in the mountainous area in central Taiwan when initial wind was from 165°, 190°, or 225°. Higher wind speed from south in the low level could cause the precipitation system to move northward away from Taiwan rather than eastward as was observed.

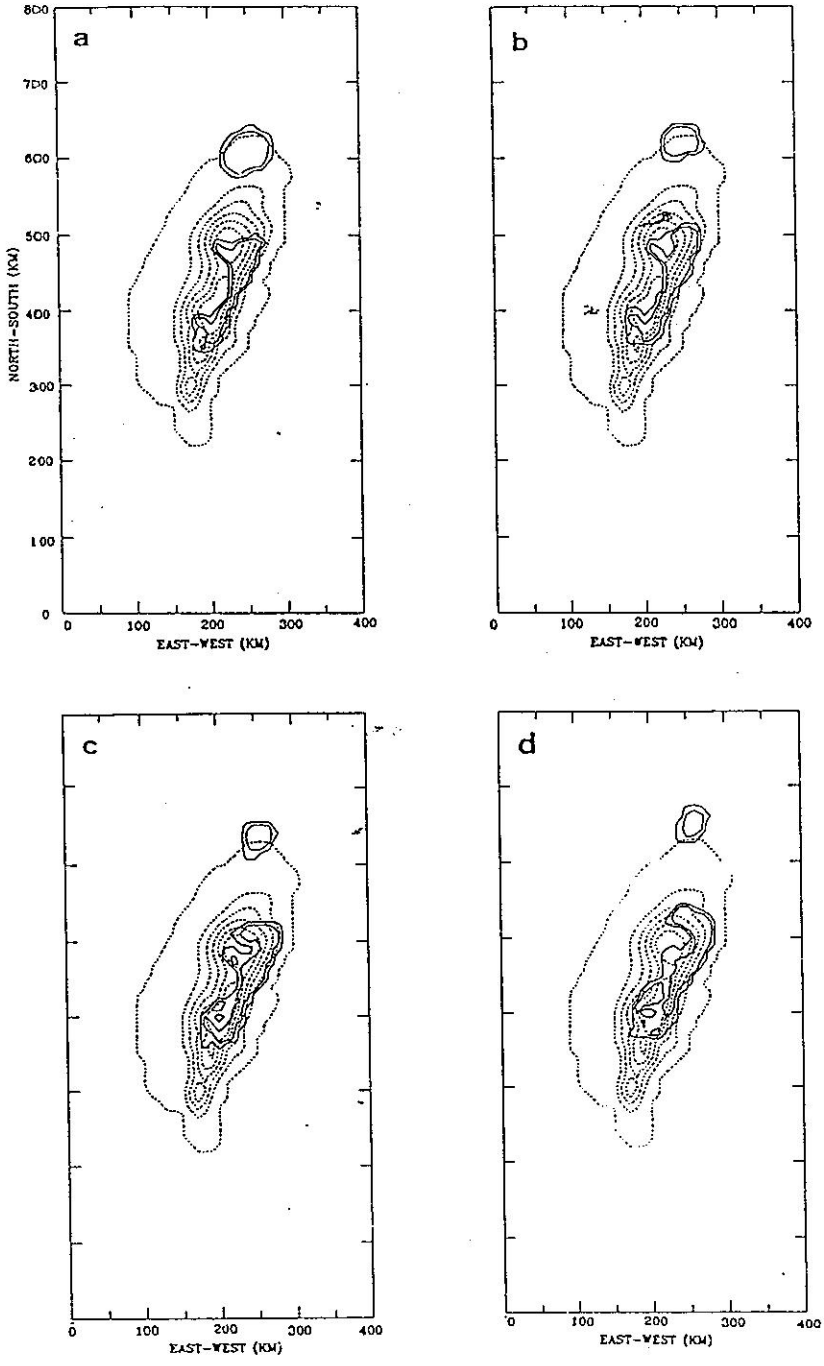

Fig. 21. Same as in Figure 14 but for run F.

More cases studies about the relationship between the formation of precipitation systems and wind direction are needed. The position of the formation of the precipitation system is sensitive to the direction of wind assumed in the model. How to obtain the "representative wind"is needs further investigation. Thus, how to specify the initial condition in the model is the major problem in the near future.

Acknowledgments This research is supported by the National Science Council under Grant NSC-82-0202-M-008-004 and NSC-82-0618-M-008-082. The computer resources were supplied by the Institute of Atmospheric Physics and the Computer Center of National Central University.

REFERENCES

Banta, R. M., 1984: Daytime boundary-layer evolution over mountainous terrain. Part I: Observations of the dry circulations. *Mon. Wea. Rev.*, **112**, 340-356.

Banta, R. M., 1986: Daytime boundary-layer evolution over mountainous terrain. Part II: Numerical studies of upslope flow duration. *Mon. Wea. Rev.*, **114**, 1112-1130.

Banta, R. M., and C. B. Schaaf, 1977: Thunderstorm genesis zones in the Colorado Rocky Mountains as determined by traceback of geosynchronous satellite images. *Mon. Wea. Rev.*, **105**, 463-476.

Chen, C.-S., W.-S. Chen, and Z. Deng, 1991: A study of a mountain-generated precipitation system in northern Taiwan during TAMEX IOP 8. *Mon. Wea. Rev.*, **119**, 2574-2606.

Durran, D. R., and J. B. Klemp, 1982: The effects of moisture on trapped mountain lee waves. *J. Atmos. Sci.*, **39**, 2490-2506.

Johnson, R. H., and J. F. Bresch, 1991: Diagnosed characteristics of Mei-Yu precipitation systems over Taiwan during the May-June 1987 TAMEX. *Mon. Wea. Rev.*, **120**, 2540-2557.

Karr, T. W. and R. L. Wooten, 1976: Summer radar echo distribution around Limon, Colorado. *Mon. Wea. Rev.*, **104**, 728-734.

Kessler, E., 1969: On the distribution and continuity of water substance in atmospheric circulation. *Meteor. Monogr.*, **32**, Am. Meteor. Soc., 84pp.

Klemp, J. B., and R. B. Wilhelmson, 1978: The simulation of three-dimensional convective storm dynamics. *J. Atmos. Sci.*, **35**, 1070-1096.

Kuo, J. T., and H. D. Orville, 1973: A radar climatology of summertime convective clouds in the Black Hills. *J. Appl. Meteor.*, **12**, 357-368.

Kuo, Y.-H., and G. T.-J. Chen, 1990: The Taiwan Area Mesoscale Experiment (TAMEX): An overview. *Bull. Am. Meteor. Soc.*, **71**, 488-503.

Liang, P. L., 1991: The Dual-doppler analysis of thunderstorms in northwest Taiwan during TAMEX IOP #11 — the structure and dynamics characteristics of thunderstorms. Master thesis, National Central University, 73pp.

Liao, S. Y., and C. S. Chen, 1984: The preliminary study of organized radar echo of frontal system and summertime convective systems. *Proc. Natl. Sci. Counc.*, A8, 250-266.

Lilly, D. K., 1962: On the numerical simulation of buoyant convective. *Tellus*, 14, 148-172.

Lin, Y.-L., N.-H. Lin, and R. P. Weglarz, 1992: Numerical modeling studies of lee mesolows, mesovortices and mesocyclones with application of the formation of Taiwan mesolows. *Meteor. Atmos. Phys.*, 49, 43-67.

Orlanski, I.,1976: A simple boundary condition for unbounded hyperbolic flow. *J. Computer Phys.*, 21, 251-269.

Appendix
Dynamic equation for the model

The model equations are cast in terrain-following coordinates (x,y,ξ) with

$$\xi = \frac{Z_t(Z - Z_s)}{Z_t - Z_s}, \tag{1}$$

where $Z_s = Z_s(x, y)$ is the height of the terrain above Z=0 and Z_t is the height of the model's top. Three tensor transformation terms used to describe the equations in the (x,y,ξ) coordinate system are

$$H^* = G^{\frac{1}{2}} = \frac{\partial \xi}{\partial z} = \frac{Z_t}{Z_t - Z_s}, \tag{2a}$$

$$G^{13} = \frac{\partial \xi}{\partial x}\frac{(\xi - Z_t)}{(Z_t - Z_s)}, \tag{2b}$$

$$G^{23} = \frac{\partial \xi}{\partial y}\frac{(\xi - Z_t)}{(Z_t - Z_s)}. \tag{2c}$$

Using the above expressions, the momentum equations can be written

$$\frac{\partial u}{\partial t} + C_p\bar{\theta}_v[\frac{\partial \pi}{\partial x} + G^{13}(\frac{\partial \pi}{\partial \xi})] = A\tilde{D}X + \tilde{D}_u K_m, \tag{3a}$$

$$\frac{\partial v}{\partial t} + C_p\bar{\theta}_v[\frac{\partial \pi}{\partial x} + G^{23}(\frac{\partial \pi}{\partial \xi})] = A\tilde{D}Y + \tilde{D}_v K_m, \tag{3b}$$

$$\frac{\partial w}{\partial t} + C_p\bar{\theta}_v[H^*(\frac{\partial \pi}{\partial \xi})] = A\tilde{D}Z + q[\frac{\theta}{\bar{\theta}} - 1 + 0.61(q_v - \bar{q}_v)] + \tilde{D}_w K_m, \tag{3c}$$

where

$$\theta_v = \theta(1 + 0.61 q_v), \tag{4a}$$

$$A\tilde{D}X = -u[\frac{\partial u}{\partial x} + G^{13}(\frac{\partial u}{\partial \xi})] + v[\frac{\partial u}{\partial y} + G^{23}(\frac{\partial u}{\partial \xi})] + wH^*(\frac{\partial u}{\partial \xi})\}, \tag{4b}$$

$$A\tilde{D}Y = -u[\frac{\partial v}{\partial x} + G^{13}(\frac{\partial v}{\partial \xi})] + v[\frac{\partial v}{\partial y} + G^{23}(\frac{\partial v}{\partial \xi})] + wH^*(\frac{\partial v}{\partial \xi}), \tag{4c}$$

$$A\tilde{D}Z = -u[\frac{\partial w}{\partial x} + G^{13}(\frac{\partial w}{\partial \xi})] + v[\frac{\partial w}{\partial y} + G^{23}(\frac{\partial w}{\partial \xi})] + wH^*(\frac{\partial w}{\partial \xi}), \tag{4d}$$

$$\tilde{D}_u = \frac{\partial}{\partial x}[2(\frac{\partial u}{\partial x} + G^{13}(\frac{\partial u}{\partial \xi})) - \frac{2}{3}(\frac{\partial u}{\partial x} + G^{13}\frac{\partial u}{\partial \xi} + H^*\frac{\partial w}{\partial \xi} + \frac{\partial v}{\partial y} + G^{23}\frac{\partial v}{\partial \xi})]$$

$$+G^{13}\frac{\partial}{\partial \xi}[2(\frac{\partial u}{\partial x} + G^{13}(\frac{\partial u}{\partial \xi})) - \frac{2}{3}(\frac{\partial u}{\partial x} + G^{13}\frac{\partial u}{\partial \xi} + H^*\frac{\partial w}{\partial \xi} + \frac{\partial v}{\partial y} + G^{23}\frac{\partial v}{\partial \xi})]$$

$$+\frac{\partial}{\partial y}(\frac{\partial u}{\partial y} + G^{23}\frac{\partial u}{\partial \xi} + \frac{\partial v}{\partial x} + G^{13}\frac{\partial v}{\partial \xi})$$

$$+G^{23}\frac{\partial}{\partial \xi}(\frac{\partial u}{\partial y} + G^{23}\frac{\partial u}{\partial \xi} + \frac{\partial v}{\partial x} + G^{13}\frac{\partial v}{\partial \xi})$$

$$+H^*\frac{\partial}{\partial \xi}(H^*\frac{\partial u}{\partial \xi} + \frac{\partial w}{\partial x} + G^{13}\frac{\partial w}{\partial \xi}), \tag{5a}$$

$$\tilde{D}_v = \frac{\partial}{\partial y}[2(\frac{\partial v}{\partial y} + G^{23}(\frac{\partial v}{\partial \xi})) - \frac{2}{3}(\frac{\partial u}{\partial x} + G^{13}\frac{\partial u}{\partial \xi} + H^*\frac{\partial w}{\partial \xi} + \frac{\partial v}{\partial y} + G^{23}\frac{\partial v}{\partial \xi})]$$

$$+G^{23}\frac{\partial}{\partial \xi}[2(\frac{\partial v}{\partial y} + G^{23}(\frac{\partial v}{\partial \xi})) - \frac{2}{3}(\frac{\partial u}{\partial x} + G^{13}\frac{\partial u}{\partial \xi} + H^*\frac{\partial w}{\partial \xi} + \frac{\partial v}{\partial y} + G^{23}\frac{\partial v}{\partial \xi})]$$

$$+\frac{\partial}{\partial x}(\frac{\partial u}{\partial y} + G^{13}\frac{\partial u}{\partial \xi} + \frac{\partial v}{\partial y} + G^{23}\frac{\partial v}{\partial \xi})$$

$$+G^{13}\frac{\partial}{\partial\xi}(\frac{\partial u}{\partial y}+G^{13}\frac{\partial u}{\partial\xi}+\frac{\partial v}{\partial x}+G^{23}\frac{\partial v}{\partial\xi})$$

$$+H^{*}\frac{\partial}{\partial\xi}(H^{*}\frac{\partial v}{\partial\xi}+\frac{\partial w}{\partial y}+G^{13}\frac{\partial w}{\partial\xi}), \tag{5b}$$

$$\tilde{D}_w=\frac{\partial}{\partial x}(H^{*}\frac{\partial u}{\partial\xi}+\frac{\partial w}{\partial x}+G^{13}\frac{\partial w}{\partial\xi})+G^{13}\frac{\partial}{\partial\xi}(H^{*}\frac{\partial u}{\partial\xi}+\frac{\partial w}{\partial x}+G^{13}\frac{\partial w}{\partial\xi})$$

$$\frac{\partial}{\partial y}(H^{*}\frac{\partial v}{\partial\xi}+\frac{\partial w}{\partial y}+G^{23}\frac{\partial w}{\partial\xi})+G^{23}\frac{\partial}{\partial\xi}(H^{*}\frac{\partial v}{\partial\xi}+\frac{\partial w}{\partial y}+G^{23}\frac{\partial w}{\partial\xi})$$

$$+H^{*}\frac{\partial}{\partial\xi}[2H^{*}\frac{\partial w}{\partial\xi}-\frac{2}{3}(\frac{\partial u}{\partial x}+G^{13}\frac{\partial u}{\partial\xi}+H^{*}\frac{\partial w}{\partial\xi}+\frac{\partial v}{\partial y}+G^{23}\frac{\partial v}{\partial\xi})]. \tag{5c}$$

θ is the potential temperature, q_v , q_c , and q_r are the mixing ratio of water vapor, cloud water and rain water respectively, and θ_v is the virtual potential temperature. Bars over individual variables refer to the initial undisturbed state.

In equations (3a), (3b), and (3c) the eddy mixing coefficient K_m is estimated according to Lilly (1962). The first law of thermodynamics is taken to be

$$\frac{\partial\theta}{\partial t}=-[(u\frac{\partial\theta}{\partial x}+uG^{13}\frac{\partial\theta}{\partial\xi})+(v\frac{\partial\theta}{\partial y}+vG^{23}\frac{\partial\theta}{\partial\xi})+H^{*}(w\frac{\partial\theta}{\partial\xi})]$$

$$+(\frac{\partial}{\partial x}+G^{13}\frac{\partial}{\partial\xi})[K_h(\frac{\partial\theta}{\partial x}+G^{13}\frac{\partial\theta}{\partial\xi})]+(\frac{\partial}{\partial y}+G^{23}\frac{\partial}{\partial\xi})[K_h(\frac{\partial\theta}{\partial y}+G^{13}\frac{\partial\theta}{\partial\xi})]$$

$$+H^{*}K_h(\frac{\partial}{\partial z}\frac{\partial\theta}{\partial\xi}), \tag{6}$$

where K_h is the eddy diffusivity of heat. The value of K_h is assumed to be three times of K_m in this study. The pressure equation model takes the form

$$\frac{\partial\Pi}{\partial t}+\frac{\bar{C}^2}{C_p\bar{\theta}_v}\left[\frac{\partial u}{\partial x}+G^{13}(\frac{\partial u}{\partial\xi})+\frac{\partial v}{\partial y}+G^{23}(\frac{\partial v}{\partial\xi})+\frac{H}{\bar{\rho}}\frac{\partial\bar{\rho}w}{\partial\zeta}\right]=0 \tag{7}$$

and Exner function Π is the non-dimensional pressure in the form $(\frac{P}{P_0})^{\frac{R_d}{C_p}}$. Here P_0 is the base state pressure at ground level and R_d is the gas constant for dry air. C is the speed of sound.

The mixing ratio of water vapor, q_v, mixing ratio of cloud water , q_c, and the mixing ratio of rain water, q_r, are considered in the model. The equation for q_v , q_c , q_r are

$$\frac{\partial q_v}{\partial t} = -[(u\frac{\partial q_v}{\partial x} + uG^{13}\frac{\partial q_v}{\partial \varsigma}) + (v\frac{\partial q_v}{\partial y} + vG^{23}\frac{\partial q_v}{\partial \varsigma}) + H^*(w\frac{\partial q_v}{\partial \varsigma})]$$

$$+(\frac{\partial}{\partial x} + G^{13}\frac{\partial}{\partial \varsigma})[K_h(\frac{\partial q_v}{\partial x} + G^{13}\frac{\partial q_v}{\partial \varsigma})] + (\frac{\partial}{\partial y} + G^{23}\frac{\partial}{\partial \varsigma})[K_h(\frac{\partial \theta_v}{\partial y} + G^{13}\frac{\partial q_v}{\partial \varsigma})]$$

$$+H^*\frac{\partial}{\partial \varsigma}(K_h H\frac{\partial q_v}{\partial \varsigma}) \tag{8}$$

$$\frac{\partial q_c}{\partial t} = -[(u\frac{\partial q_c}{\partial x} + uG^{13}\frac{\partial q_c}{\partial \varsigma}) + (v\frac{\partial q_c}{\partial y} + vG^{23}\frac{\partial q_c}{\partial \varsigma}) + H^*(w\frac{\partial q_c}{\partial \varsigma})]$$

$$+(\frac{\partial}{\partial x} + G^{13}\frac{\partial}{\partial \varsigma})[K_h(\frac{\partial q_c}{\partial x} + G^{13}\frac{\partial q_c}{\partial \varsigma})] + (\frac{\partial}{\partial y} + G^{23}\frac{\partial}{\partial \varsigma})[K_h(\frac{\partial \theta_c}{\partial y} + G^{13}\frac{\partial q_c}{\partial \varsigma})]$$

$$+H^*\frac{\partial}{\partial \varsigma}(K_h H\frac{\partial q_c}{\partial \varsigma}) \tag{9}$$

$$\frac{\partial q_r}{\partial t} = -[(u\frac{\partial q_r}{\partial x} + uG^{13}\frac{\partial q_r}{\partial \varsigma}) + (v\frac{\partial q_r}{\partial y} + vG^{23}\frac{\partial q_r}{\partial \varsigma}) + H^*(w\frac{\partial q_r}{\partial \varsigma})]$$

$$+(\frac{\partial}{\partial x} + G^{13}\frac{\partial}{\partial \varsigma})[K_h(\frac{\partial q_r}{\partial x} + G^{13}\frac{\partial q_r}{\partial \varsigma})] + (\frac{\partial}{\partial y} + G^{23}\frac{\partial}{\partial \varsigma})[K_h(\frac{\partial \theta_c}{\partial y} + G^{13}\frac{\partial q_r}{\partial \varsigma})]$$

$$+H^*\frac{\partial}{\partial \varsigma}(K_h H\frac{\partial q_r}{\partial \varsigma}) \tag{10}$$

參考文獻

丘台光與劉復誠，1985：民國年月日台灣北部地區豪雨之個案研究，大氣科學，12，93 - 102 .

王陳台琦、林沛綠、陳景森、楊健生與魏逐寶梅雨期中尺度對流系統產生豪雨的雷達分析.天氣分析與預報研討會.227 - 238 . 台北 .

Chen,C.S.,and S.M.Lin.1983:A study of the lateral boundary condition in a numerical storm model. Bull.Geophys.,National. Central Univ., ROC, 24, 57-76.

Durran,D.R.,and J.B.Klemp,1982:The effects of mostiure on trapped mountain lee waves. *J. Atmos. Sci.*, 39, 2490-2506.

Doswell Ⅲ, C.A., 1986 : Short - range forecasting . 689 - 719 . Mesoscale meteorology and forecasting . American Meteorological Society . Edited by Ray .

Gal-Chen,T.,and R.Somerville,1975:Numerical solution of the Navier-stokes equation with topography. *J. Comput. Phys.*, 17, 209-223.

Johnson,R.H., and J.Bresch.,1991:Diagnosed characteristics of preciption systems over Taiwan during the May-June 1987 TAMEX.*Mon. Wea. Rev.*,119, 2540-2557.

Klemp,J.B.,and R.B Wilhelmson,1978:The simulation of three dimensional convective storm dynamics.*J.Atmos.Sci.*, 35, 1070-1096.

Liao , S - Y and C - S cahe ,1984 : The preliminary study of organized radar echo of frontal systems and of summertime convective systems . Proceedings of the National Science Councvl . Part A . , 8 , 250 - 266 .

Lin ., P - L , T - C Chen Wang , and C - C Yeh , 1989 : Doppler observational study of a long - lived rabinband in TAMEX . IOP - 13 . Papers in Meteorological Research , 12 , 91 - 120 .

Mc Ginley . J . 1986 : Nowcasting mesoscale phenomena . 657 - 688 . Mesoscale meteorology and forecasting . American Meteorological Society . Edited by Ray.